# Supplementary Material

## Hybrid lipid/block copolymer vesicles display broad phase coexistence region

Naomi Hamada[a], Sukriti Gakhar[a], and Marjorie L. Longo*[a]

[a] Department of Chemical Engineering, University of California Davis, Davis, California 95616, United States
*Email: mllongo@ucdavis.edu

**Table of contents:**



## S1. Comparisons to DPPC/DOPC

DPH anisotropy values and the absolute value of their derivatives in DPPC/DOPC LUVs were evaluated as a function of temperature (

Figure S1A and S1B) to provide a comparison to DPPC/PBd-PEO LUVs.

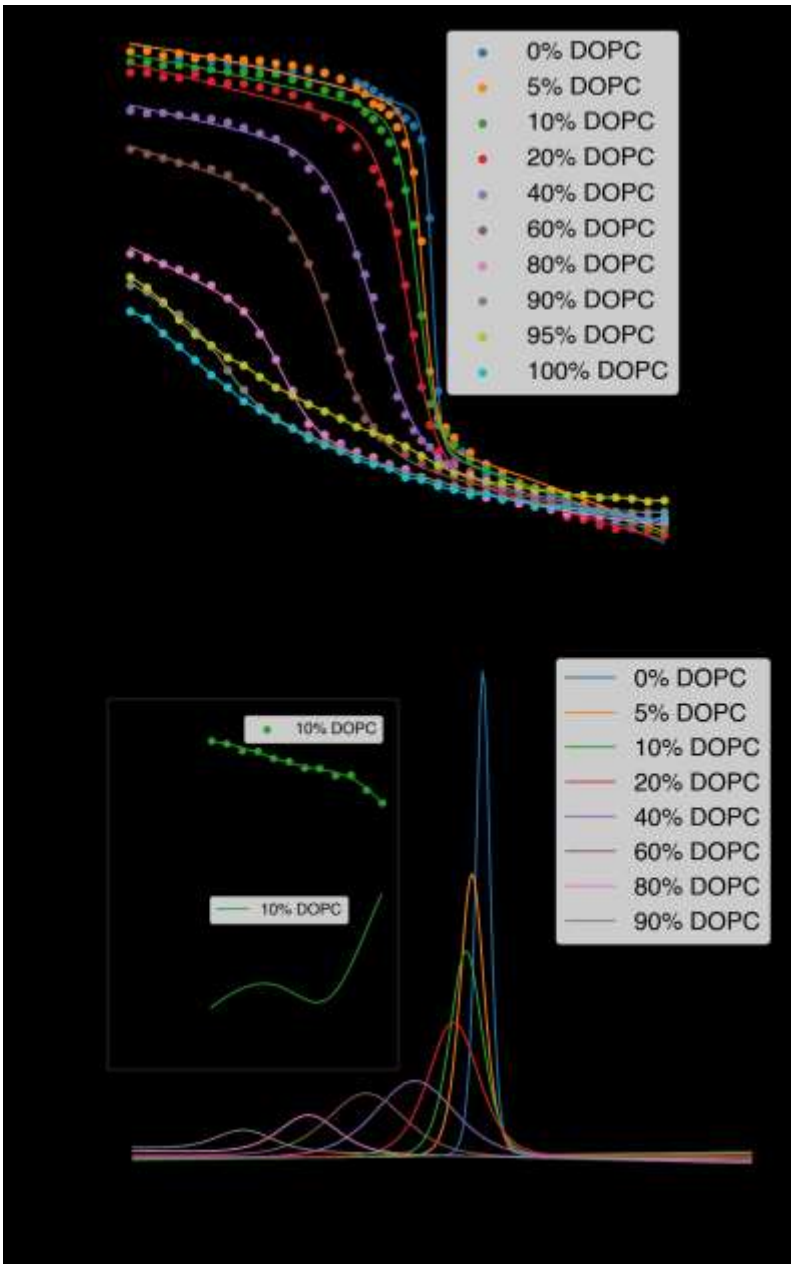


Figure S1. A. Anisotropy (r) of DPH in DPPC/DOPC LUVs as a function of temperature. Plotted lines show sigmoidal fit to measured anisotropy values as described in the main text (Section 2.3), except for LUVs containing 95% or 100% DOPC. Equation 2 (main text, Section 2.3) could not be regressed for these compositions due to the lack of clear inflection point. Plotted lines for 95% and 100% DOPC are not the result of any fit. B. Absolute values of the derivatives of the regressed curves in A with respect to temperature. Inset shows the same sigmoidal fit applied to 10% DOPC LUVs from 4-26 $^{o}$C, the temperature range within which the transition of DOPC from the solid to the fluid phase is expected. The fit yielded a $T_{mid}$ of 10.9 $^{o}$C, corresponding to the maximum of the absolute value of the

first derivative of the fit with respect to temperature.

Figure S2 compares $T_{completion}$ of DPPC/DOPC, DPPC/18:2 PC, DPPC/18:3 PC, and DPPC/PBd-PEO vesicles. S, S+F, and F indicate regions where solid, solid and fluid, and fluid phases exist or coexist. Solid domains are DPPC-rich. $T_{completion}$ was obtained from DPH anisotropy for DPPC/DOPC, DPPC/18:2 PC, and DPPC/18:3 PC LUVs and from DPH anisotropy and laurdan GP for DPPC/PBd-PEO LUVs.

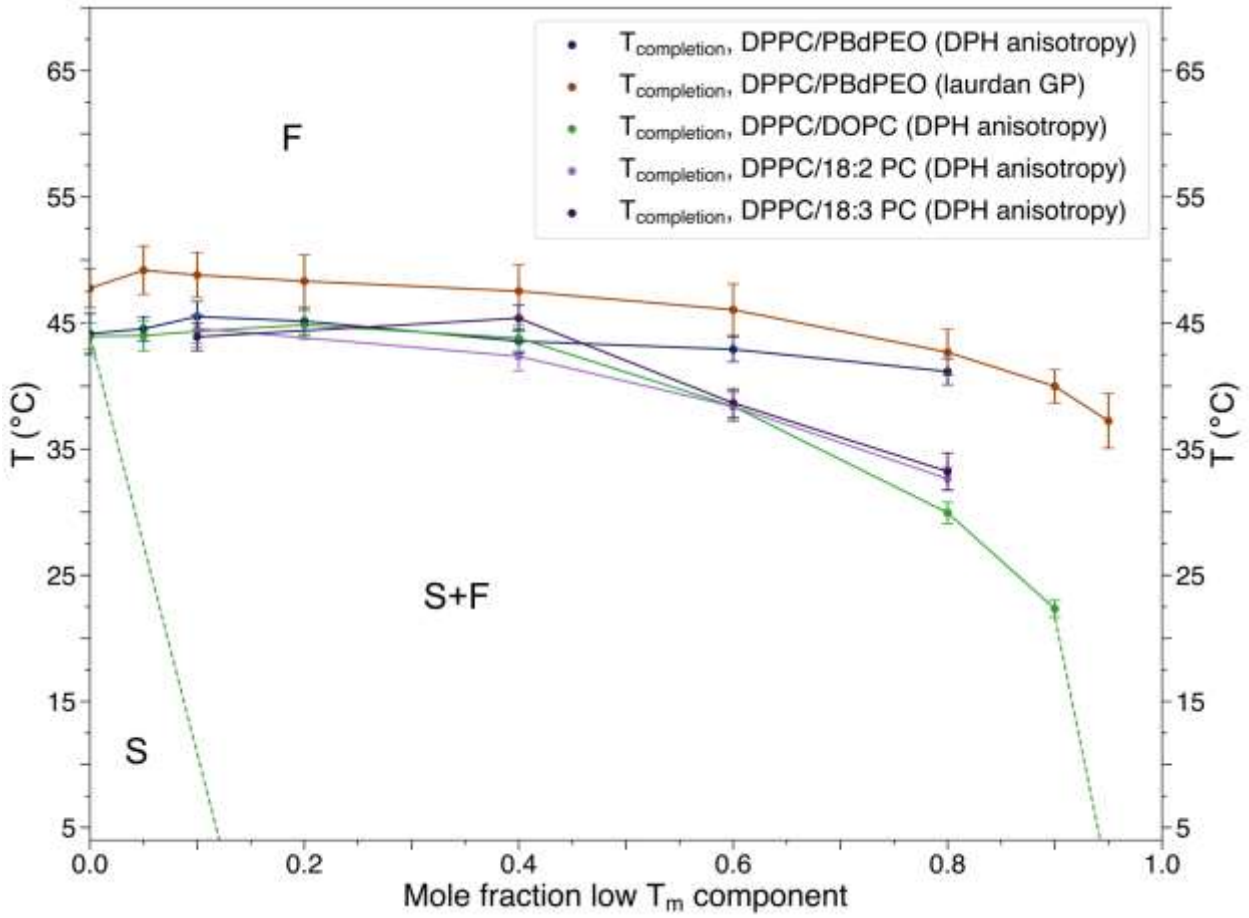


Figure S2. Comparison between $T_{completion}$ for DPPC/DOPC, DPPC/18:2 PC, DPPC/18:3 PC, and DPPC/PBd-PEO LUVs. The *x*-axis corresponds to the mole fraction of DOPC for DPPC/DOPC LUVs, or to the mole fraction of PBd-PEO for PBd-PEO/DPPC LUVs. The left dashed green line represents the left side of the DPPC/DOPC solidus line based on the $T_{mid}$ of 10.9 °C as an estimate for the solidus transition in 10% DOPC LUVs (see lower inset of Figure S1B). The right dashed green line is an estimated continuation of the DPPC/DOPC liquidus line, drawn based on a solid-fluid transition temperatureof -20 °C for pure DOPC [1,2]. Error bounds for $T_{completion}$ were determined as the difference between the intersection of tangent lines to the points of steepest slope and of greatest curvature for the absolute value of the first derivative of the anisotropy or GP values for each composition. For 100% DPPC, this uncertainty was propagated for 3 samples; for all other samples, plotted values represent data from one sample. Error bars correspond to two times the propagated standard deviation error from three samples (100% DPPC DPH anisotropy data) or two times the standard deviation error from one sample (all other data) for the value of $T_{mid}$ returned from regression of measured DPH anisotropy or GP values against a sigmoidal function as described in "Methods" in the main text (Section 2.3).

For comparison, the data presented in Figure S1 using LUVs were also analyzed using the calculations described by Lentz et al. [2,3] (Figure S3). Using this method, the delimiting temperatures of the phase transition correspond to breakpoints in the dependence of the apparent viscosity of the membrane. According to the phase diagram of Lentz et al. [2], the onset ($T_{low}$) and completion ($T_{high}$) temperatures decrease nearly linearly with vesicle composition for multilamellar vesicles (MLVs). However, three delimiting temperatures were reported for small unilamellar vesicles (SUVs) of each composition. For SUVs, the completion temperature decreases first slowly, then more rapidly as increasing amounts of DOPC are incorporated.

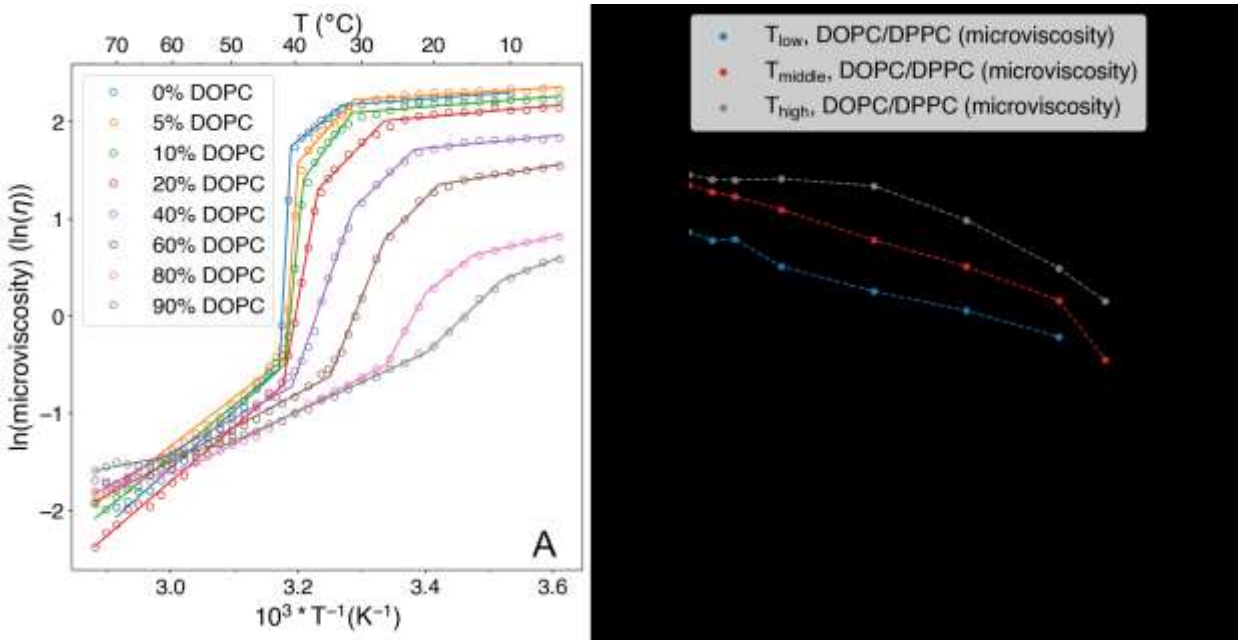


Figure S3. A. Temperature dependence of the natural logarithm of the apparent microviscosity of DPPC/DOPC LUVs, calculated as previously described [2,3] from the data shown in Figure S1. B. Breakpoints in the temperature dependence of microviscosity values shown in A, corresponding to the method previously used [2] to assess the delimiting temperatures of the phase transition.

Applying the methods of Lentz et al. [2,3] to the data in Figure S1 yielded Figure S3A. The profiles in Figure S3B shared characteristics with the phase diagrams published by Lentz et al. [2] for MLVs and for SUVs. Three distinct breakpoints ($T_{low}$, $T_{middle}$, $T_{high}$) in the dependence of apparent membrane viscosity with temperature were evident in the vicinity of the phase transition for the LUVs examined here, similar to the trends previously reported for SUVs. The shape of the completion temperature line was similar to that previously reported for SUVs. However, the shape of the onset line was most similar to that previously reported for MLVs. Therefore, the profiles shared properties with both the MLV and SUV phase diagrams, perhaps due to the characteristics LUVs share with both MLVs and SUVs (i.e. reduced curvature strain in comparison to SUVs and unilamellarity, respectively). Similarly, the completion temperatures in Figure S3A are within a couple of

degrees of those previously reported for SUVs below 60% DOPC and MLVs above 60% DOPC.

## S2. Effects of vesicle preparation and measurement methods on $T_{mid}$

The effects of various sample preparation methods on $T_{mid}$ were investigated (Figure S4) at both 80% and 90% DOPC in DPPC/DOPC vesicles. Vesicle type and preparation methods vary across both of the previously published phase diagrams and the work presented here. Schmidt et al. constructed a phase diagram using MLVs in potassium phosphate buffer prepared from ethanol (EtOH)-based lipid stock solution [1], while Lentz et al. reported phase diagrams for MLVs and SUVs prepared from chloroform-based lipid stock solutions in a potassium chloride solution [2]. Factors such as vesicle suspension medium [4,5] and vesicle curvature and lamellarity [6,7] have been previously reported to impact bilayer mechanical properties and phase behavior to varying extents. The factors investigated here were therefore: vesicle type (LUV or MLV), lipid stock solution solvent (chloroform or EtOH), rehydration medium (20 mM Tris/100 mM NaCl buffer or water), LUV preparation method (freeze-thawed prior to extrusion, or extruded after hydration at ~50 $^{o}$C), direction of temperature ramp during measurement (heating or cooling), and DPH:lipid ratio (1:30 or 1:500). If it is stated that vesicles were passed through freeze-thaw cycles prior to extrusion, lipid thin films of the desired composition were prepared as described in “Methods” in the main text (Section 2.2), hydrated at 50 $^{o}$C, and subjected to five freeze-thaw cycles (5 minutes at -65 $^{o}$C, 5 minutes at 50 $^{o}$C). LUVs were then prepared by extrusion.

Slight variations in $T_{mid}$ were observed for vesicles of differing lamellarity and sample preparation methods (

Table S1), and it is possible that some of the factors investigated may genuinely impact $T_{mid}$. For example, vesicle preparation in water instead of Tris/NaCl buffer generally corresponded to a slightly increased $T_{mid}$, suggesting the choice of buffer may have some effect on phase behavior. Very slight differences between $T_{mid}$ values for DPPC vesicles of varying curvature and lamellarity have also been previously reported [6], and similar behavior is observed here as well. When averaged across preparation methods, 80% DOPC LUVs had a $T_{mid}$ of (23.02±0.30) $^{o}$C, while 80% DOPC MLVs had a $T_{mid}$ of (22.87±0.90) $^{o}$C. Similarly, 90% DOPC LUVs had a $T_{mid}$ of (17.50±1.16) $^{o}$C, while 90% DOPC MLVs had a $T_{mid}$ of (17.50±1.18) $^{o}$C. Further work would be required to draw

definitive conclusions, however, as the standard deviation of $T_{mid}$ observed here for both compositions (~0.6-1.2 °C) is consistent with a variation in vesicle composition of ~1-2% (within the range of experimental error) due to the strong dependence of $T_{mid}$ on composition for vesicles containing large amounts of DOPC. This suggests the $T_{mid}$ reported in this work did not depend strongly on the sample preparation methods used, though slight variation is still possible.

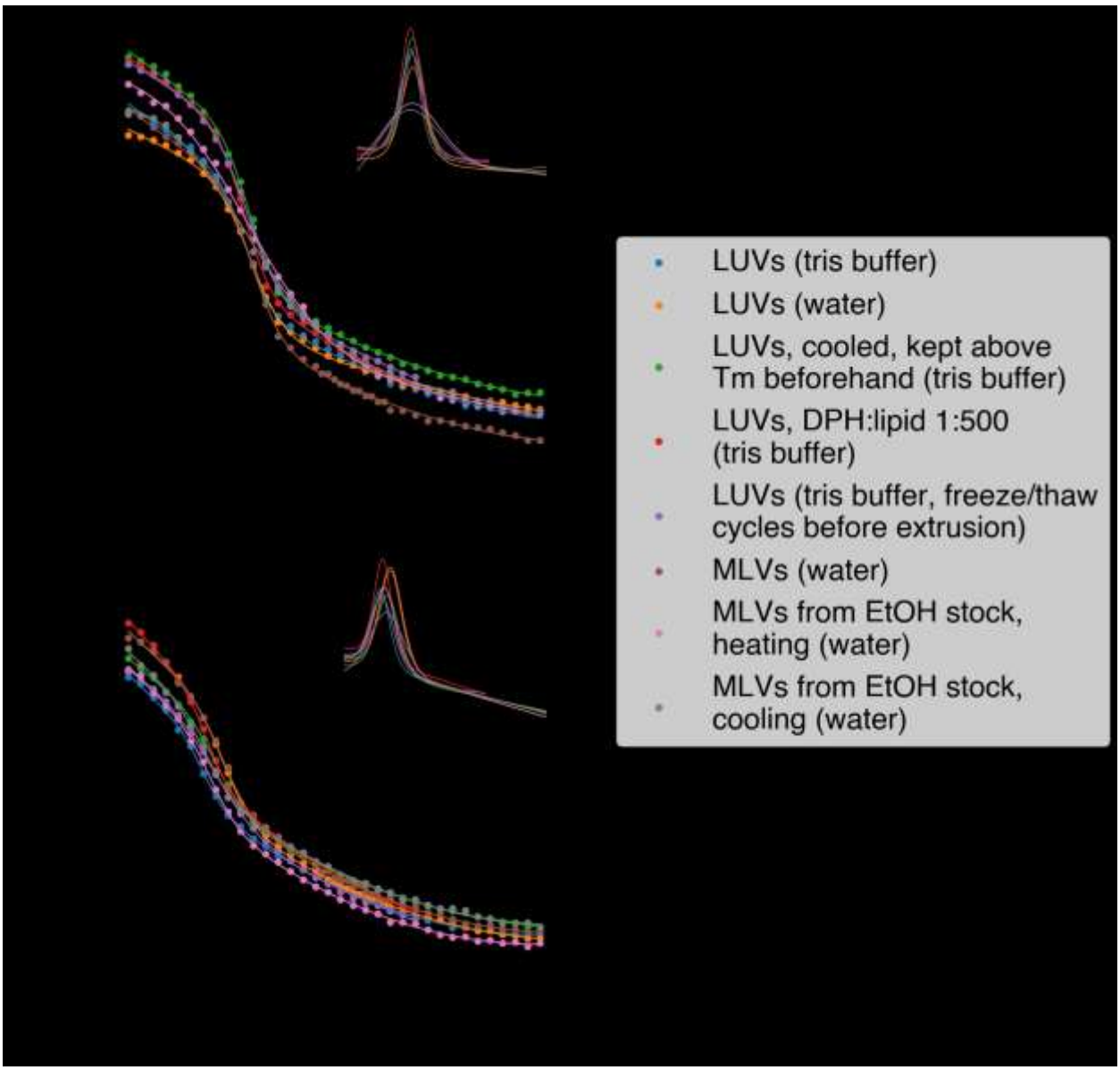


Figure S4. Dependence of DPH anisotropy values on vesicle preparation methods and lamellarity for DPPC/DOPC vesicles containing A. 80% DOPC or B. 90% DOPC. Insets show absolute values of the first derivatives of each DPH anisotropy curve with respect to temperature.

Table S1. Vesicle preparation conditions and corresponding $T_{mid}$ values for DPPC/DOPC vesicles containing either 80% or 90% DOPC. A DPH:lipid ratio of 1:30 was used for all samples unless otherwise specified. Final row reports mean $T_{mid}$ value and standard deviation.

| **Sample** | **80% DOPC, $T_{mid}$ (°C)** | **90% DOPC, $T_{mid}$ (°C)** |
|---|---|---|
| LUVs in 20 mM Tris/100 mM NaCl (chloroform lipid stock, measured from 4-70 °C) | 22.8 | 15.8 |
| LUVs in water (chloroform lipid stock, measured from 4-70 °C) | 23.4 | 19.1 |
| MLVs in water (chloroform lipid stock, measured from 4-70 °C) | 23.9 | 19.1 |
| MLVs in water (EtOH lipid stock, measured from 4-70 °C) | 23.0 | 17.1 |
| MLVs in water (EtOH lipid stock, measured from 70-4 °C) | 21.7 | 16.3 |
| LUVs in 20 mM Tris/100 mM NaCl (chloroform lipid stock; extruded from freeze-thawed MLVs and measured from 4-70 °C) | 23.0 | 17.9 |
| LUVs in 20 mM Tris/100 mM NaCl (chloroform lipid stock; maintained above $T_{mid}$ until use and measured from 70-4 °C) | 23.3 | 18.1 |
| LUVs in 20 mM Tris/100 mM NaCl (chloroform lipid stock; measured from 4-70 °C; DPH:lipid ratio 1:500) | 22.6 | 16.6 |
| **Average** | 22.96±0.62 | 17.50±1.16 |

Figure S5 demonstrates the reversibility of DPH anisotropy with temperature in 40:60 DPPC:PBd-PEO LUVs. The difference in $T_{mid}$ observed between heating and cooling cycles was small (0.4 °C), suggesting the temperature ramp rate used for fluorescence experiments was sufficiently slow to permit sample equilibration.

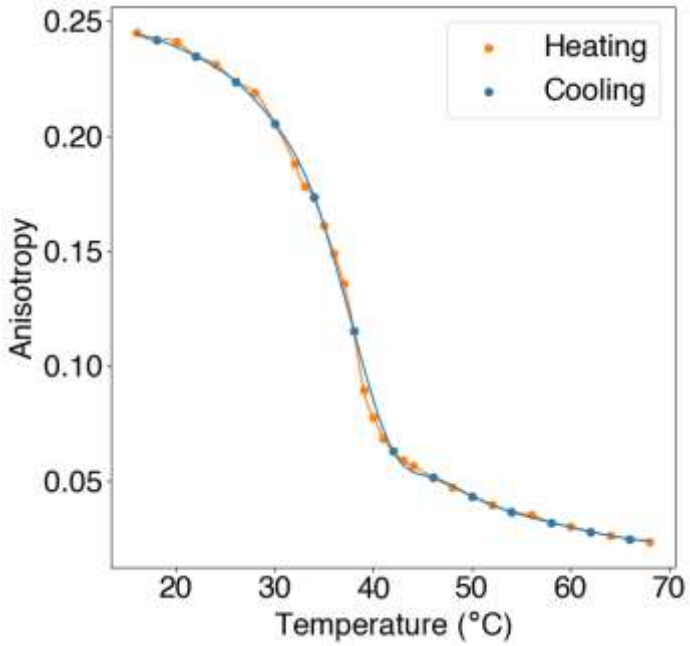


Figure S5. DPH anisotropy in 40:60 DPPC:PBd-PEO LUVs. Sample was heated from 16-70 ˚C to obtain "Heating" curve, then cooled at the same rate from 70-16 ˚C to obtain "Cooling" curve.

DPH anisotropy in hybrid LUVs containing different DPH:lipid/polymer ratios was also evaluated to ensure DPH concentration did not significantly affect the observed behavior (Figure S6). DPH:(DPPC+PBd-PEO) ratios of 1:30 and 1:500 were evaluated for 80:20 DPPC:PBd-PEO LUVs. The observed $T_{mid}$ agreed within 0.4 ºC, suggesting no significant alteration of membrane behavior between the two DPH concentrations.

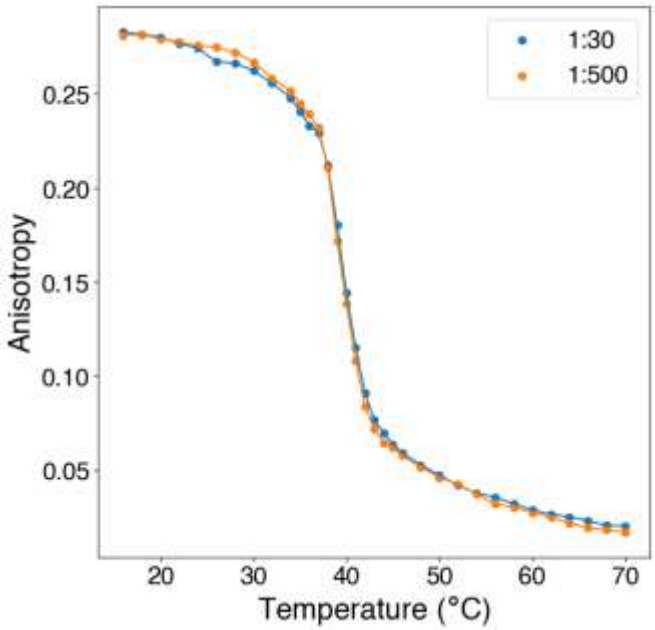


Figure S6. Comparison between DPH anisotropy curves obtained with different DPH:(DPPC+PBd-PEO) molar ratios. Legend indicates this ratio. Data shown for 80:20 DPPC:PBd-PEO LUVs.

## S3. Deviations from ideal fluidity

To gain further insight into the dependence of membrane fluidity on vesicle composition, the deviation of DPH anisotropy values from those predicted for the case of ideal mixing was determined [8]. Ideal anisotropy values ($r_{ideal}$) were calculated as functions of temperature and composition as shown in Equation (S1), corresponding to the weighted sum of the anisotropy values observed in the pure DPPC ($r_{DPPC}$) and pure PBd-PEO ($r_{PBdPEO}$) LUVs. $x_{DPPC}$ and $x_{PBdPEO}$ are the mole fractions of DPPC and PBd-PEO.

$$r_{ideal} = x_{DPPC} r_{DPPC} + x_{PBdPEO} r_{PBdPEO} \quad \text{(S1)}$$

The deviation of observed anisotropy values from ideal values, $\Delta r/r$, was calculated as shown in Equation (S2) and plotted as a function of vesicle composition across a range of temperatures (Figure 2 in the main text). Positive values of $\Delta r/r$ suggest the LUV membrane is less fluid than would be expected if it were ideally mixed, as membrane fluidity is inversely proportional to DPH anisotropy values.

$$\frac{\Delta r}{r} = \frac{r_{actual} - r_{ideal}}{r_{ideal}} \quad \text{(S2)}$$

A plot of $\Delta r/r$ for DPPC/DOPC vesicles (Figure S7) also displays visible trends differentiating temperatures above and below $T_{completion}$, though not always as distinct as those observed for the DPPC/PBd-PEO system. Below $T_{completion}$, where solid and fluid DPPC-rich and DOPC-rich phases coexist for a wide range of vesicle compositions, primarily positive deviations from ideality are observed, similarly to the DPPC/PBd-PEO system. Larger negative deviations from ideality are also observed at temperatures close to $T_{completion}$ for most compositions in both DPPC/DOPC and DPPC/PBd-PEO vesicles. Above $T_{completion}$, however, primarily smaller, negative deviations from ideal anisotropy values are observed for DPPC/DOPC vesicles (as opposed to the clearly negative deviations from ideality observed for DPPC/PBd-PEO vesicles). This difference is likely due to the similarity of the fluidities of DPPC and DOPC above their $T_{mid}$, which would limit the dependence of $\Delta r/r$ on vesicle composition. Indeed, the anisotropy values of pure DPPC and pure DOPC are within ~0.01 anisotropy units of each other above 50 °C (

Figure S1). DPPC/DOPC membrane fluidity might thus be expected to display only weak deviations from ideality above $T_{completion}$. Conversely, DPPC and PBd-PEO display appreciably different anisotropy values even above the $T_{mid}$ of DPPC (ranging from 0.04-0.02 for pure DPPC and 0.09-0.05 for pure PBd-PEO as the temperature varies from 50-70 °C), indicating PBd-PEO is more ordered than fluid DPPC. Greater dependence of fluidity on composition and thus potentially larger deviations from ideality would therefore be possible for DPPC/PBd-PEO LUVs. This could contribute to the more distinct trends

in *Δr/r* observed above $T_{completion}$ for DPPC/PBd-PEO vesicles as compared to DPPC/DOPC vesicles.

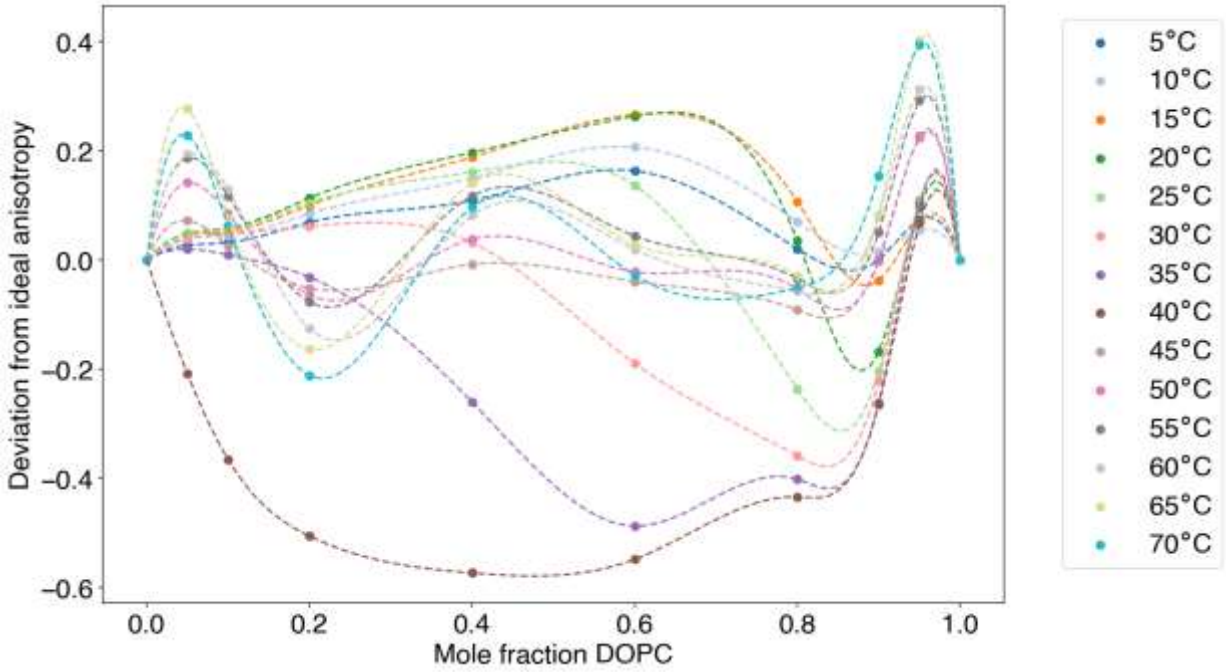


Figure S7. Deviations from ideal anisotropy (*Δr/r)* for DPPC/DOPC LUVs. Points were calculated as described above (with PBd-PEO replaced by DOPC); dashed lines are cubic splines fit to calculated values.

## S4. Effects of fluorescent probe Rh-DOPE on $T_{mid}$

To investigate the potential of Rh-DOPE to impact the $T_{mid}$ reported by FRET, DPH anisotropy and laurdan GP were used to evaluate $T_{mid}$ for LUVs containing 1% or 2% Rh-DOPE (to match the concentrations used for FRET experiments), as shown in Figure S8. $T_{mid}$ values were relatively similar in LUVs made with and without Rh-DOPE (Table S2), especially in comparison to the significant differences between $T_{mid}$ reported by FRET and by DPH anisotropy/laurdan GP. $T_{mid}$ values increased slightly upon inclusion of Rh-DOPE.

The differences in the shapes of the anisotropy and GP curves between LUVs made with and without Rh-DOPE may be the result of FRET, as both DPH and laurdan can participate in FRET with Rh-DOPE. GP may be especially strongly impacted by this, as GP values are calculated by comparing laurdan emission intensities at two different wavelengths (440 nm and 490 nm). The latter is closer to the excitation peak of rhodamine, so laurdan emission at 490 nm may be more strongly quenched by participation in FRET with rhodamine than at 440 nm. This would result in elevated GP values, as greater differences between laurdan emission intensity values at 440 nm and 490 nm correspond to higher GP.

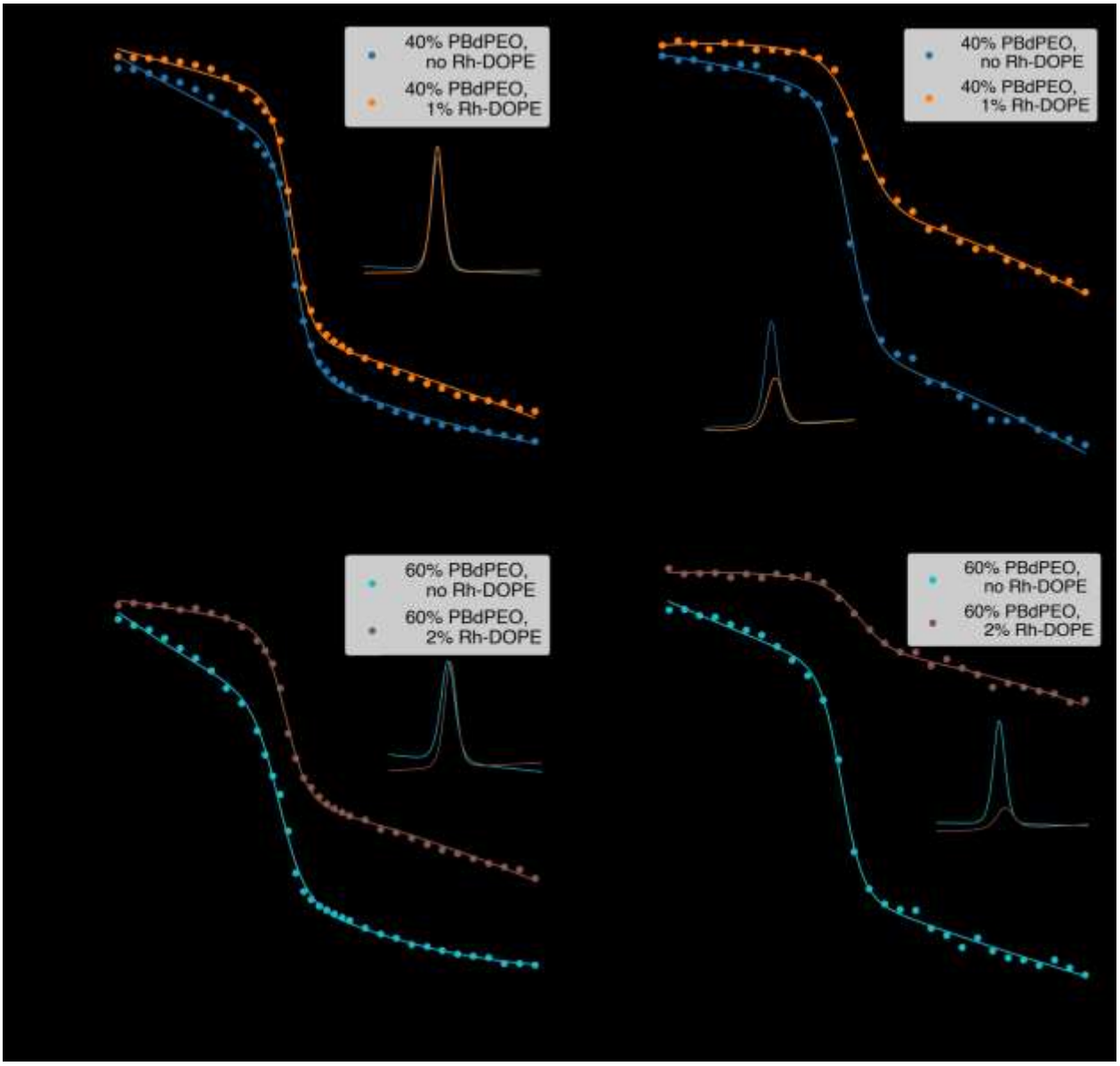


Figure S8. DPH anisotropy and laurdan GP in 60:40 and 40:60 DPPC:PBd-PEO LUVs in the presence and absence of 1% and 2% Rh-DOPE, respectively (matching the percentage used for FRET experiments with vesicles of each composition). Insets show the absolute values of the derivatives of the DPH anisotropy and laurdan GP curves with respect to temperature. DPH anisotropy and laurdan GP curves were fit using the sigmoidal expressions described in "Methods" in the main text (section 2.3).

Table S2. Comparison of $T_{mid}$ values reported by DPH anisotropy and laurdan GP in LUVs made with and without Rh-DOPE. $\Delta T_{mid}$ refers to the differences in $T_{mid}$ for LUVs made with and without the indicated amount of Rh-DOPE; positive values indicate $T_{mid}$ was greater for LUVs containing Rh-DOPE.

| | **DPH anisotropy $\Delta T_{mid}$ (°C)** | **Laurdan GP $\Delta T_{mid}$ (°C)** |
|---|---|---|
| 1% Rh-DOPE | +0.5 | +1.34 |
| 2% Rh-DOPE | +0.9 | +2.2 |

## S5. Light scattering measurements of LUV size

The average diameters of extruded hybrid LUVs were determined by dynamic light scattering and are shown in Table S3.

Table S3. Diameters of DPPC/PBd-PEO LUVs indicated by DLS. Uncertainty represents standard deviation of at least 4 measurements.

| Mole fraction PBd-PEO | LUV diameter (nm) |
|---|---|
| 0 | 113±9 |
| 0.05 | 120±12 |
| 0.2 | 86±9 |
| 0.4 | 98±11 |
| 0.6 | 80±5 |
| 0.8 | 96±13 |
| 0.9 | 90±10 |
| 0.95 | 117±3 |
| 1 | 95±18 |

## S6. Assessment of $T_{onset}$, $T_{mid}$, $T_{completion}$

### *0.1. DPH anisotropy*

$T_{mid}$ was determined from DPH anisotropy values by least squares regression to a sigmoidal function in Python as described in "Methods" in the main text (Section 2.3). $T_{onset}$ and $T_{completion}$ correspond to the start and end of the peak in the absolute value of the derivative of this function with respect to temperature (Figure S9). The baseline was determined by fitting a straight line along the base of either side of the peak. Tangent

lines were constructed against the steepest point of the sides of each peak and against the points of greatest curvature (visually determined) as the derivative returned to its baseline on each side. The points at which these tangent lines intersect with the baseline were averaged to obtain $T_{onset}$ and $T_{completion}$. The error bounds on $T_{onset}$ and $T_{completion}$ were then the differences between the points at which the lines on each side of the peak intersects with the baseline (i.e. for $T_{onset}$, the difference between the points at which the two green lines constructed along the left side of the peak intersect with the baseline).

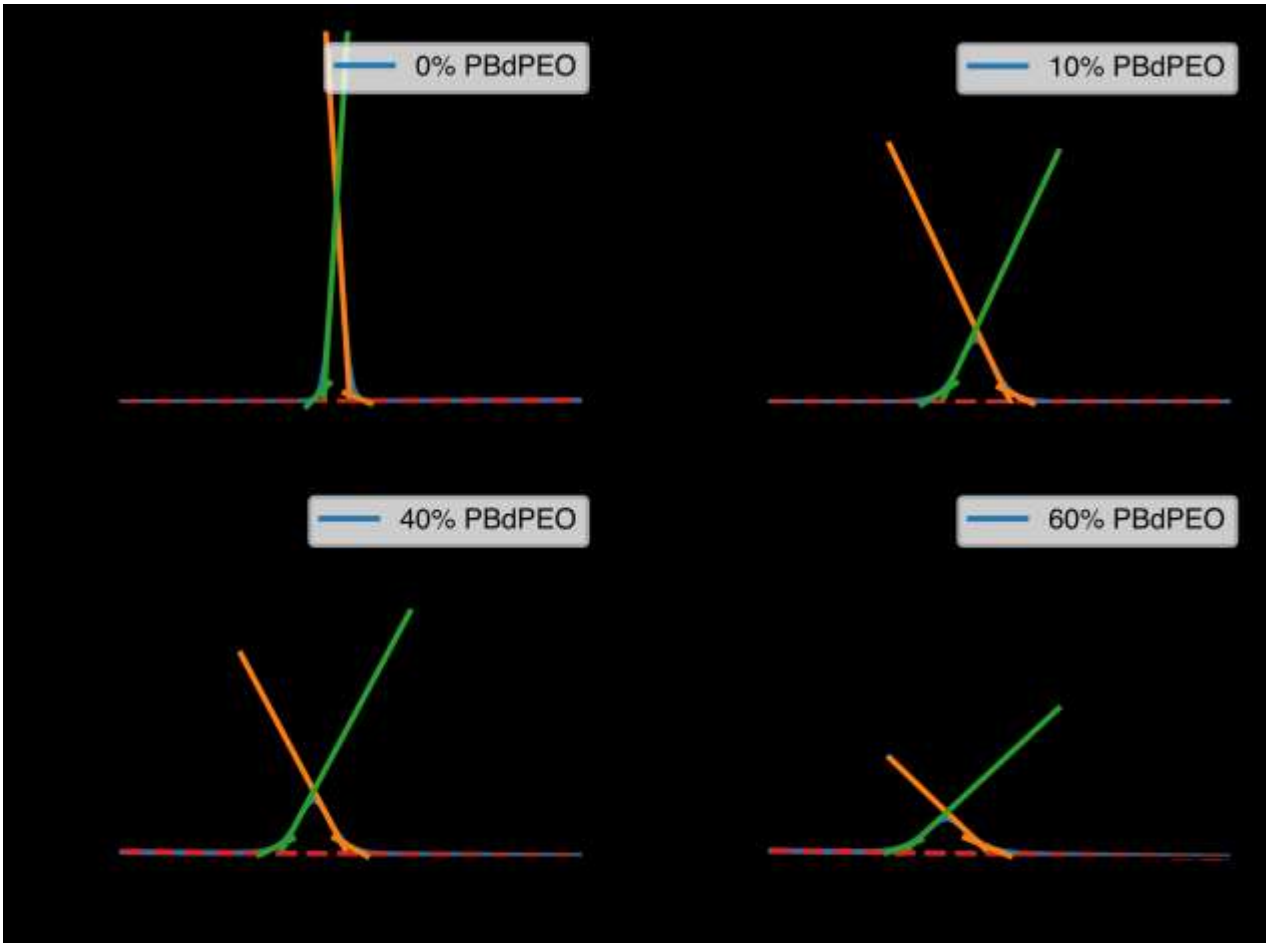


Figure S9. Representative plots of the absolute values of the first derivatives of the sigmoidal function to which DPH anisotropy values were fitted, along with tangent constructions and fitted baseline (red) used to determine $T_{onset}$ and $T_{completion}$. The mean of the intersection with the baseline of lines tangent to the points of steepest slope and of greatest curvature was taken as $T_{onset}$ (green) or $T_{completion}$ (orange).

### *0.2. Laurdan GP*

The observed GP values were regressed against a sigmoidal function as described in "Methods" in the main text (Section 2.3). $T_{mid}$ was thus determined as a regression parameter of the sigmoidal fit. $T_{onset}$ and $T_{completion}$ were evaluated by taking the absolute

value of the derivative with respect to temperature of the fit to the observed GP values and constructing tangents as described for DPH anisotropy values. Representative derivatives and tangents are shown in Figure S10.

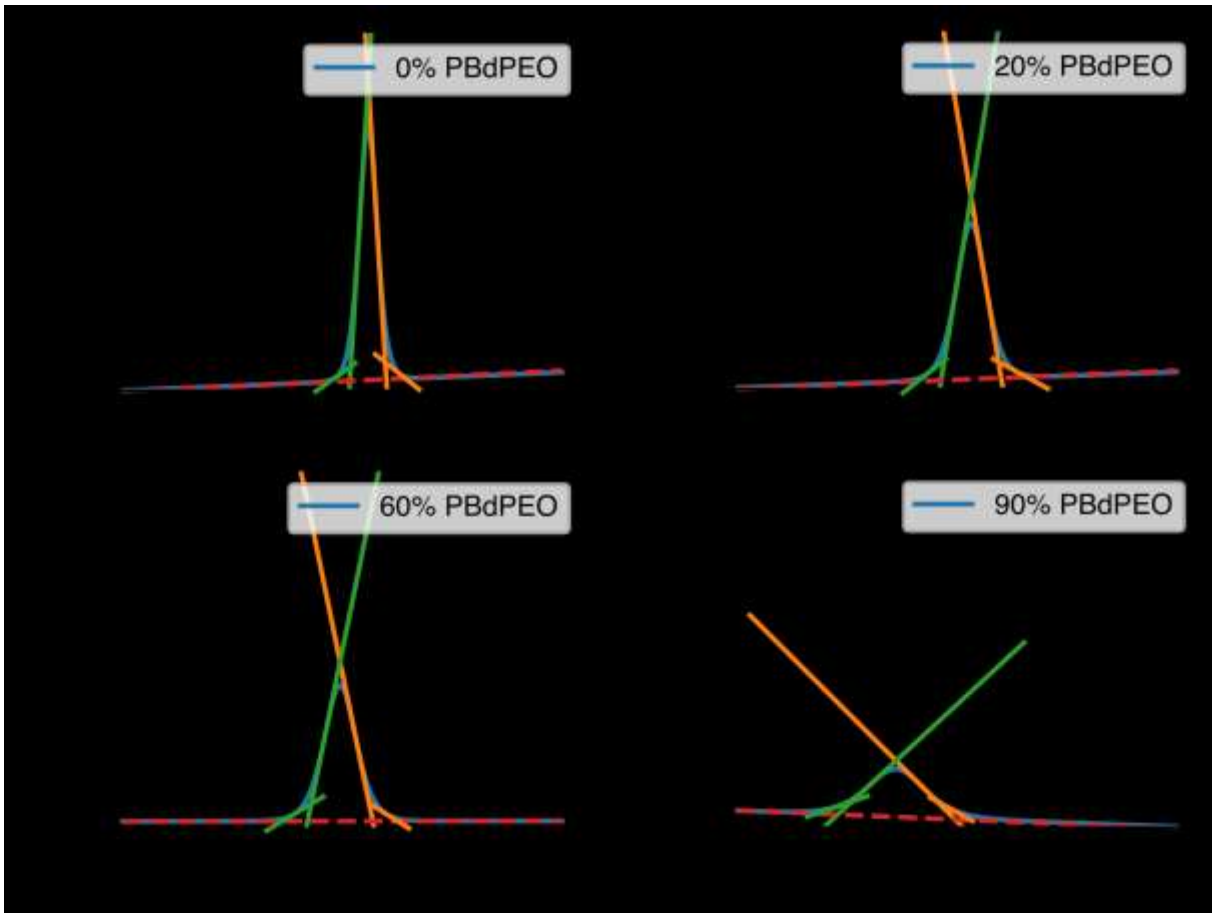


Figure S10. Sample tangent constructions for plots of the absolute value of the derivative of laurdan GP with respect to temperature for DPPC/PBd-PEO LUVs. The mean of the intersection with the baseline of lines tangent to the points of steepest slope and of greatest curvature was taken as $T_{onset}$ (green) or $T_{completion}$ (orange).

### *S6.3. Statistical analysis*

For single samples, $T_{mid}$ uncertainty values were determined by doubling the standard deviation error for $T_{mid}$ obtained by least squares regression of measured anisotropy or GP values against the sigmoidal functions described in “Methods” (Section 2.3 in the main text). If it is specified that multiple samples were measured to obtain a mean $T_{mid}$ and corresponding uncertainty value, the reported $T_{mid}$ is the average obtained from at least 3 independent samples, each independently regressed against a sigmoidal function. The uncertainty in this average $T_{mid}$ is the propagated error in the average using the standard deviation errors of $T_{mid}$ across at least 3 samples. This propagated error was doubled for error bounds and error bars.

Although multiple anisotropy measurements were taken per sample per temperature, the uncertainties arising from variation in multiple measurements on the same sample were not included because the standard deviation of anisotropy measurements on the same sample was typically ~2 orders of magnitude smaller than the standard deviation across samples.

References:


[1] M.L. Schmidt, L. Ziani, M. Boudreau, J.H. Davis, Phase equilibria in DOPC/DPPC: Conversion from gel to subgel in two component mixtures, The Journal of Chemical Physics. 131 (2009) 175103. https://doi.org/10.1063/1.3258077.

[2] B.R. Lentz, Y. Barenholz, T.E. Thompson, Fluorescence depolarization studies of phase transitions and fluidity in phospholipid bilayers. 2. Two-component phosphatidylcholine liposomes, Biochemistry. 15 (1976) 4529–4537. https://doi.org/10.1021/bi00665a030.

[3] M. Shinitzky, Y. Barenholz, Fluidity parameters of lipid regions determined by fluorescence polarization, Biochimica et Biophysica Acta (BBA) - Reviews on Biomembranes. 515 (1978) 367–394. https://doi.org/10.1016/0304-4157(78)90010-2.

[4] R.L. Knorr, J. Steinkühler, R. Dimova, Micron-sized domains in quasi single-component giant vesicles, Biochimica et Biophysica Acta (BBA) - Biomembranes. 1860 (2018) 1957–1964. https://doi.org/10.1016/j.bbamem.2018.06.015.

[5] H. Bouvrais, L. Duelund, J.H. Ipsen, Buffers Affect the Bending Rigidity of Model Lipid Membranes, Langmuir. 30 (2014) 13–16. https://doi.org/10.1021/la403565f.

[6] M.A. Kreutzberger, E. Tejada, Y. Wang, P.F. Almeida, GUVs Melt Like LUVs: The Large Heat Capacity of MLVs Is Not Due to Large Size or Small Curvature, Biophysical Journal. 108 (2015) 2619–2622. https://doi.org/10.1016/j.bpj.2015.04.034.

[7] N. Kučerka, J. Pencer, J.N. Sachs, J.F. Nagle, J. Katsaras, Curvature Effect on the Structure of Phospholipid Bilayers, Langmuir. 23 (2007) 1292–1299. https://doi.org/10.1021/la062455t.

[8] M.M. Lozano, M.L. Longo, Complex formation and other phase transformations mapped in saturated phosphatidylcholine/DSPE-PEG2000 monolayers, Soft Matter. 5 (2009) 1822. https://doi.org/10.1039/b820070j.